

Water Self-Dissociation is Insensitive to Nanoscale Environments

Solana Di Pino^a, Yamila A. Perez Sirkin^a, Uriel N. Morzan^b, Verónica M. Sánchez^a, Ali Hassanali^{b,1}, Damian A. Scherlis^{a,1},

a. Departamento de Química Inorgánica, Analítica y Química Física/INQUIMAE, Facultad de Ciencias Exactas y Naturales, Universidad de Buenos Aires, Buenos Aires, Argentina

b. International Centre for Theoretical Physics, Trieste, Italy

¹ E-mail: ahassana@ictp.it or damian@qi.fcen.uba.ar.

Abstract

Nanoconfinement effects on water dissociation and reactivity remain controversial, despite their importance to understand the aqueous chemistry at interfaces, pores, or aerosols. The pK_w in confined environments has been assessed from experiments and simulations in a few specific cases, leading to dissimilar conclusions. Here, with the use of carefully designed *ab-initio* simulations, we demonstrate that the energetics of bulk water dissociation is conserved intact to unexpectedly small length-scales, down to aggregates of only a dozen molecules or pores of widths below 2 nm. The reason is that most of the free-energy involved in water autoionization comes from breaking the O-H covalent bond, which has a comparable barrier in the bulk liquid, in a small droplet of nanometer size, or in a nanopore in the absence of strong interfacial interactions. Thus, dissociation free-energy profiles in nanoscopic aggregates or in 2D slabs of 1 nm width reproduce the behavior corresponding to the bulk liquid, regardless of whether the corresponding nanophase is delimited by a solid or a gas interface. The present work provides a definite and fundamental description of the mechanism and thermodynamics of water dissociation at different scales with broader implications on reactivity and self-ionization at the air-liquid interface.

Introduction

Confinement deeply affects the physical chemistry of water. In cavities or pores of a few nanometers, its freezing point can drop as much as 50°C [19, 29, 38], while other dynamic and thermodynamic properties such as diffusivity [4, 14, 26, 40, 46], dielectric constant [8, 27, 28, 37], melting enthalpy [12, 21], or thermal expansion [22, 49], experience significant changes. Remarkable progress has been made in the investigation of water at the nanoscale regime: spectroscopic and calorimetric techniques [2, 4, 14, 21, 26, 36, 38, 46] hand in hand with molecular simulations [5, 11, 17, 27, 28, 40, 43, 45, 51], have been ingeniously applied to probe and characterize the structure, dynamics, and phase transitions of water in nanometric domains.

Notwithstanding these achievements, the role of confinement on chemical reactivity is barely understood, mostly because of the complexity associated with the determination of equilibrium and kinetic constants in these conditions. In particular, the dissociation of water in porous media, tiny aerosols, biomolecular pockets, membranes, and other nanospaces, represents a fundamental problem of extreme relevance for experimentalists, which remains unsettled. Studies in nanodroplets, reverse micelles, and cavities within supramolecular assemblies, all strongly suggest that chemical kinetics is substantially affected with respect to the bulk phase, producing accelerations of up to 6 orders of magnitude in some cases [6, 9, 13, 24, 47, 50]. This has prompted researchers to focus on confined chemistry in the search of alternative routes

for chemical synthesis [6, 9, 13, 50], to elucidate chemical transformation in the atmosphere [52], or to explain enzymatic catalysis in living organisms [23, 42]. Whereas the mechanisms behind these increased rates are still a matter of debate, the main causes that have been postulated include the over-concentration of reagents, extreme pH changes, or interfacial and entropic effects. Among the latter, the equilibrium constants of products, reagents, and solvent, all become critical [35]. Understanding how water dissociation is affected in nanoenvironments together with its role in aqueous reactivity is thus a key pending question.

Speculations based on indirect experimental evidence and theoretical conceptions have been made on a possible enhancement of the aqueous acidity in nanocavities [33]. In a recent NMR study, on the other hand, a single H₂O molecule confined in the pocket of a C₆₀ derivative was shown to be less acidic than bulk water [15]. In any case, the effect of pore radius and of the nature of the interface on the dissociation constant of water continues to be a basic question still unanswered from a general perspective. Hence, simulations become essential and have in fact contributed a number of clues that shed light on this matter.

First-principles simulations proved useful to calculate the pK_w in bulk [20, 41, 44], and were also applied to investigate the autoionization in confinement in various settings, from the interlayer spaces of minerals to carbon nanotubes [25, 31, 39]. In particular, Muñoz-Santiburcio and Marx computed the self-dissociation constant in slit pores of 1 nm delimited by FeS layers, at high temperature and pressure [31]. They claimed that the free-energy barrier to dissociation (ΔG_d) experienced a reduction of more than 15%, explained in terms of an increase in the dielectric constant arising from confinement.

In the present study, we use *ab-initio* molecular simulations in combination with an appropriate sampling coordinate to track how the water dissociation barrier is affected by system size, hence providing a general answer to the puzzle on whether and by how much the self-dissociation of water changes as the dimensions of the liquid phase approaches the nanometer. We formulate and respond the question of how big the aqueous domain must be to preserve the energetics and the mechanism of bulk water dissociation. The answer is surprising: an aqueous cluster of just a dozen molecules exhibits a dissociative free-energy profile that cannot be distinguished from the one corresponding to the bulk phase. Size effects only start to tally in an aggregate that has half this number of molecules, or in pores of widths below 1.6 nm, where solvation of the hydronium and hydroxide ions are severely hindered. Our work rationalizes this outcome with the help of data-science tools, and manages to reconcile previous, apparently contradictory findings, offering a comprehensive picture of water dissociation at the nanoscale. Beyond its obvious impact on chemistry under confinement, the results of our simulations have broader implications on how the pK_w changes near hydrophobic interfaces such as the surface of water or aqueous solutions.

Results and discussion

Dissociation barrier of nanoconfined water

The dissociation free energy of water in the bulk phase was first computed from *ab-initio* molecular simulations in the late 90's by Trout and Parrinello [44], employing density functional theory (DFT). These authors adopted the O-H distance of the dissociating bond as the reaction coordinate. While this constraint proved to be appropriate to induce bond breaking and to form the ion pair, when the O-H separation exceeds a certain length, it can not prevent the recombination of the hydroxide with a different proton through Grotthuss diffusion [41], and therefore the application of this scheme seems to be unable to produce a well separated OH⁻-H₃O⁺ pair. Shortly after,

Sprick proposed the proton coordination n_H as an alternative reaction coordinate that, by avoiding recombination, may facilitate the separation of the ions [41]. This variable, implemented in some of the studies cited in the introductory section [25, 31, 39], counts the number of protons surrounding a given oxygen atom. Each H atom contributes to n_H with a quantity that varies continuously between 0 and 1, depending on the O-H distance (see Supporting Information). Thus, the proton coordination assumes fractionary values and can be used to introduce a bias potential that enforces dissociation in a particular H_2O molecule as n_H changes from 2 to 1.

Very recently, the study of water dissociation from *ab-initio* simulations was extended to two dimensional sampling by combining the coordination number with the donor-acceptor distance [20]. These calculations have contributed what is possibly the most accurate thermodynamic landscape for bulk water dissociation available so far. In comparing 2D with 1D sampling, however, the author noticed that the latter, when based on the coordination number, yields a sufficiently accurate profile for a model of 64 molecules. In the light of this precedent, we perform here one-dimensional sampling using the proton coordination, which allows us to afford the large number of computationally intensive calculations arising from the different model systems considered in this work. We emphasize that for the present investigation the precise value of ΔG_d is not as relevant as it is its dependence on system dimensions. For bulk water our methodology reproduces the free-energy profiles reported from previous molecular dynamics simulations using comparable schemes [25, 31, 39, 41, 44]. These approaches tend to underestimate the experimental dissociation free-energy by a few kcal/mol, which is ascribable to the DFT functionals. Importantly, however, our conclusions are not tied to the energy barriers resulting from the calculations, dependent on the particular numerical scheme. Instead, they rely on the variation of these barriers as a function of system size, ostensibly more robust. The fact that the main outcome of the present analysis is grounded on the changes in the dissociative barrier rather than on the barrier itself, makes it pretty much independent of the DFT functional or electronic structure method chosen, and is a major strength of this study. In the Supporting Information we include results establishing that the level of theory employed herein accurately captures these changes in the reaction energies arising from alterations in the solvation structure, which is the critical asset in the present context. These benchmark calculations show that our quantum-mechanical approach, while remaining computationally efficient to undertake the large number of calculations involved, can reliably describe such effects.

Using this strategy, we computed the barrier to dissociation for isolated water clusters of 6, 12, and 20 molecules of H_2O at 298 K. The results are presented in Figure 1, together with the curve corresponding to bulk water at the same temperature. Something remarkably surprising happens: the free energy profile for the aggregate of 12 molecules, with an average diameter not larger than 1 nm, does not differ, within the error of the method, from the one obtained for the system of 20 molecules, and the two of them are in turn indistinguishable from the curve corresponding to the bulk phase. Since the dissociation of water creates two ions, it can be expected that their solvation energy would be strongly modulated by the size of the hydrogen bond network. Instead, a change in the barrier is only observed for the smallest system consisting of 6 molecules, where ΔG_d increases by nearly 30%.

A similar trend is found for water in slit nanopores. The dissociation barrier was studied at 298 K for water confined between graphene layers separated by 0.94, 1.2, and 1.6 nm. The smallest of these pore models is represented in Figure 2c. We employed for these simulations a multiscale quantum-mechanics molecular-mechanics (QM-MM) scheme [18, 39] where the graphene plates were described with an atomic force-field, and the aqueous phase with DFT (see details in Supporting Information). The use of this

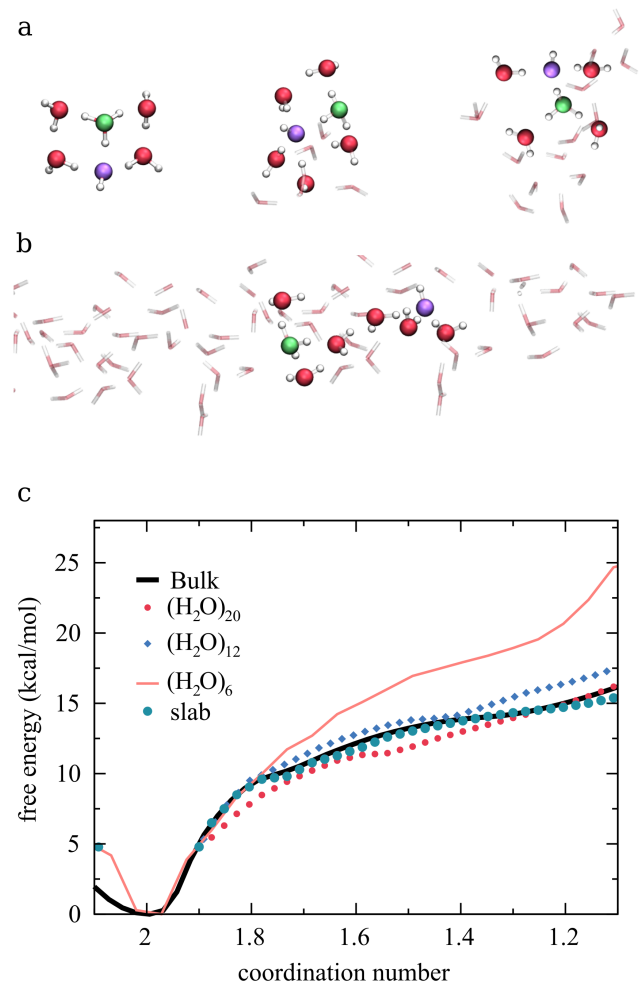


Figure 1. **a:** Snapshots of the (H₂O)₆, (H₂O)₁₂, and (H₂O)₂₀ clusters illustrating the product (dissociated) state. Oxygen atoms belonging to the OH⁻ and H₃O⁺ ions are shown in blue, including the hydrogen-bonded molecules in a balls-and-sticks depiction. **b:** Periodic model for the water slab of width 1 nm. **c:** Free energy profiles computed for the dissociation of water in the bulk phase, and for the model systems represented above. The coordination number alludes to the proton coordination of the oxygen atom in the donor water molecule.

treatment has a twofold motivation: whereas it makes affordable the large number of large-scale simulations needed to complete the analysis, it also offers the possibility of tuning the water-wall interaction, hence providing a way to assess the effect of hydrophobicity. We have considered two different interactions that produce weakly hydrophilic and moderately hydrophobic contact angles (θ) of 42° and 86° respectively. [48] The interlayer space was filled according to the water content determined from classical molecular dynamics simulations of graphene pores immersed in an aqueous liquid reservoir in contact with a gas phase. The reservoir was thermalized at 298 K and was exposed to a vacuum region to mimic the air-water interface, thus reproducing ambient conditions (see Supporting Information).

The free-energy curves corresponding to a water-graphene contact angle of 42° , displayed in Figure 2a, reveal the same behavior that was observed for the water aggregates: a spacing of just 1.6 nm is enough to recover the bulk limit. A very similar result is obtained for $\theta=86^\circ$, suggesting that the effect is inherent to confinement regardless of the affinity for the interface, at least in the absence of specific interactions (see Supporting Information). The density profiles presented in Figure 2b show an excluded volume involving a fringe of more than 2 Å adjacent to each graphene plate, leaving in the smallest pores accessible interlayer spaces of only ~ 0.5 nm and ~ 0.7 nm respectively, comparable to the dimensions of the $(\text{H}_2\text{O})_6$ cluster. The effective width in the 1.6 nm pore reaches nearly a nanometer, closer to the size of the $(\text{H}_2\text{O})_{12}$ structure, which seems to be sufficient to restore the bulk dissociation barrier.

This unanticipated outcome, i.e., the insensitivity of water dissociation with respect to system size, is consistent with the data from *ab-initio* simulations presented by Liu and coworkers, showing that in 1.5 nm slit pores of layered neutral clay models, K_w was essentially the same as in bulk water [25]. These authors reported that the acidity was increased in the presence of interstitial Mg^{2+} cations, while remaining almost unaltered in a neutral environment, attributing to the charge, and not the confinement itself, the rise in K_w . On the other hand, this seems to be at odds with the more recent work from Marx’s group [31], ascribing to bidimensional confinement in slit pores of 1 nm, an enhancement of $55\times$ in the self-dissociation constant K_w . This disagreement is rather puzzling, given that they share the same methodology, based on DFT Car-Parrinello molecular dynamics and the proton coordination n_H as the reaction coordinate. The origin of this apparent contradiction, however, can be easily tracked to the water content implemented in each of these simulations. A critical aspect to get meaningful barriers, contrastable with the bulk values, is the filling of the nanopores, because the dissociation free energy depends on the pressure, which is extremely sensitive to the amount of water inside the model pore unit cell. In the *NVT* simulations by Muñoz-Santiburcio and Marx, the density, and not the pressure, was the thermodynamic variable under control [31]. In particular, the number of water molecules N filling the pore was fixed to yield a target density ρ , with $N = \rho \times V_{eff}$, where V_{eff} was arbitrarily chosen. This resulted in an overcompression of the fluid with respect to the target pressure (see the Supporting Information for details) that produced the observed enhancement in K_w attributed to a confinement effect—the dissociation constant of water is known to grow as a function of pressure [3]. In fact, those simulations recovered the bulk value of the pK_w when ρ was reduced by 35% (Figure 3 in ref. [31]). In the study by Liu et al., [25] instead, or in our own simulations, the number of water molecules included in the supercell was equilibrated with a reservoir at ambient pressure.

To corroborate this interpretation, we applied the same protocol to compute the water dissociation free-energy in an extended slab of 1 nm width in the vacuum at 298 K. This slab consisted of 32 H_2O molecules contained in a supercell of lateral dimensions $14.69 \times 14.69 \text{ \AA}^2$, approximately the same as those used in ref. [31]. These

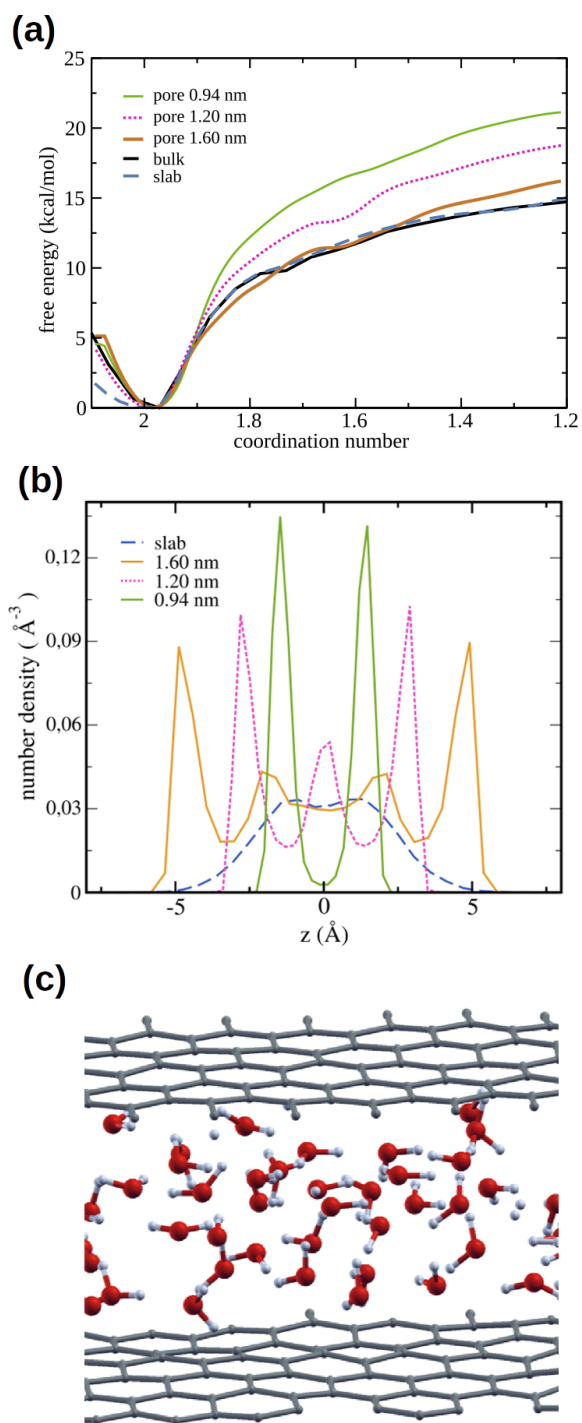


Figure 2. a: Free-energy profiles computed for water dissociation within slit pores of different widths, delimited by graphene layers of moderate hydrophilicity ($\theta=42^\circ$). The profiles corresponding to bulk water and a 1 nm periodic slab in the gas phase are also given for comparison. **b:** Water density profiles as a function of the spatial coordinate perpendicular to the principal axis, for the pores and the slab. **c:** Model of the slit pore of graphene, of width 0.94 nm.

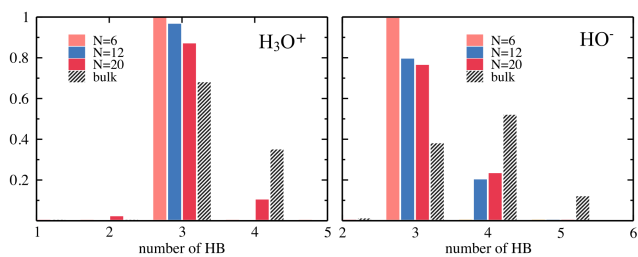


Figure 3. Distribution of the number of hydrogen bonds formed by the hydronium and the hydroxide ions in the clusters and in the bulk phase.

simulations recreate the conditions of bidimensional confinement, avoiding any compression effects—since the water structure can equilibrate with the gas phase—and suppressing the interactions with the pore walls. In this way, the emerging free-energy profile expresses the sole effect of 2D confinement. This profile is depicted in Figures 1 and 2a, where it can be seen that ΔG_d turns out to be—within the error of our method—not different from the one corresponding to the bulk liquid.

The question that naturally arises is: what is the rationale for the observed trend in the pK_w? A simple explanation can be given in terms of the hydrogen bond structure. The dissociation free-energy is determined by the thermodynamic stability of the products, hydronium and hydroxide, which will in turn depend on the ability of the hydrogen bond network to solvate these ions. Figure 3 summarizes the information regarding the number of hydrogen bonds in the clusters and in the bulk, showing that the OH⁻ anion loses one hydrogen bond in the smallest cluster with respect to the rest of the environments. In the bulk phase, the hydroxide accepts 4 strong hydrogen bonds and donates a weak one [1]. A detailed analysis of the hydrogen bond network, as the one provided in Table 1, reveals that in the 6 molecules aggregate, and also in the pore of 0.94 nm, the hydroxide accepts only 3 hydrogen bonds, while it accepts up to 4 in all the other systems. This missing bond appears to be the reason for its destabilization and the rise in the barrier when $N=6$, or when the interstitial spacing is 1.20 nm or less. Moreover, the hydronium ion donates 3 strong and accepts one weak hydrogen bond in the bulk. In the clusters and in the narrowest pore the latter interaction is lost, however this does not appear to significantly affect the thermodynamics of dissociation. The fact that the oxygen of the hydronium is rather hydrophobic [1] can explain why placing it in a small cluster does not incur a large energetic cost. The hydrogen bond distribution shows in the smallest pore a more complex behavior than in the clusters: in the former, the distribution is broader, with the number of H-bonds varying from 1 to 5. The net effect is in any case the loss of one of the strong bonds of the OH⁻ anion, similarly to what is observed for the cluster of 6 molecules. In the larger pore, instead, the hydrogen bond network around the ions resembles that of bulk water (see Supporting Information for a discussion on the hydrogen bond network).

What it takes to drive the ions apart

Up to now, the rationalization of the dissociation free energy has namely involved the energetic contribution of breaking the covalent bond and the reorganization of hydrogen bonding. Nevertheless, once the ions are formed, they must separate away from each other creating solvent screened entities. The underlying mechanism by which this happens and the corresponding thermodynamics has been a topic of lively discussion in the literature. First-principles simulations by Geissler and co-authors have shown that the stabilization of the products in the autoionization of water requires the ions to be separated by at least three bonds; in that situation, a fluctuation that

Table 1. Average distribution of hydrogen bonds for the hydroxide and hydronium species.

		donates	accepts
BULK	H ₃ O ⁺	3	1
	OH ⁻	1	3-4
N=20	H ₃ O ⁺	3	0
	OH ⁻	0	3-4
N=12	H ₃ O ⁺	3	0
	OH ⁻	0	3-4
N=6	H ₃ O ⁺	3	0
	OH ⁻	0	3
SLAB	H ₃ O ⁺	3	0
	OH ⁻	0	3-4
pore 0.94 nm	H ₃ O ⁺	3	0
	OH ⁻	0	3
pore 1.60 nm	H ₃ O ⁺	3-4	1
	OH ⁻	1	3-4

interrupts the “hydrogen bond wire” facilitates the diffusion of the proton through the Grotthuss mechanism, thus leading to the effective separation of the hydroxide and hydronium species [10]. More recent work by Hassanali and co-workers has shown the hydrogen bond wire undergoes collective compressions which are essential for the proton transfer and hydronium-hydroxide separation [16]. Using machine-learning approaches, van Erp and co-workers proposed that besides the wire compression, factors such as the alignment of the hydrogen bond wire and the extent of tetrahedrality of the water molecules also play important roles [30].

In the clusters, their own size restrains the maximum separation that the ions can attain. The average hydroxide-hydronium distances (d_{12}) fluctuate around 2.5-3.5 Å during the molecular dynamics sampling in the different aggregates (Supporting Information), reflecting that these ionic species are rarely separated by more than one hydrogen bond. This behavior is also observed in the bulk: the trajectories show that even for the lowest values of n_H , the hydroxide and the hydronium tend to reside not further than two bonds apart, and that they may even be in contact most of the time. The dimensions of the supercell are in principle large enough to enable a separation between the counterions of up to five hydrogen bonds, or $d_{12} \sim 8$ Å. The fact that distances beyond 4 Å are seldom explored suggests that the use of n_H as the reaction coordinate may not be effective to create fully solvated and decorrelated hydronium and hydroxide ions. It is thus reasonable to wonder whether our computations are missing an additional contribution to the free energy associated with a further delocalization of the ions that may account for a difference between the bulk and the confined systems.

To enforce a full separation of the ions, a new reaction coordinate can be defined composed of the proton coordination of two different, distant oxygen atoms, $n_H(1)$ and $n_H(2)$. By setting the reaction coordinate as the difference between these two, $\xi(\Delta n_H) = n_H(2) - n_H(1)$, and sampling the phase space from $\xi=0$ to $\xi=2$, it is possible to drive a proton from a given water molecule (containing oxygen 1) to another chosen molecule (containing oxygen 2) lying far away, thus producing a well separated OH⁻-H₃O⁺ pair. The distance between these two water molecules may slightly vary during the process, however, their diffusion is negligible within the elapsed time.

Figure 4a presents the free energy resulting from this scheme (blue curve) with oxygens 1 and 2 initially separated by ~ 8 Å. In addition, the profile obtained earlier is also shown in red on the right panel for easy comparison. To interpret the free-energy

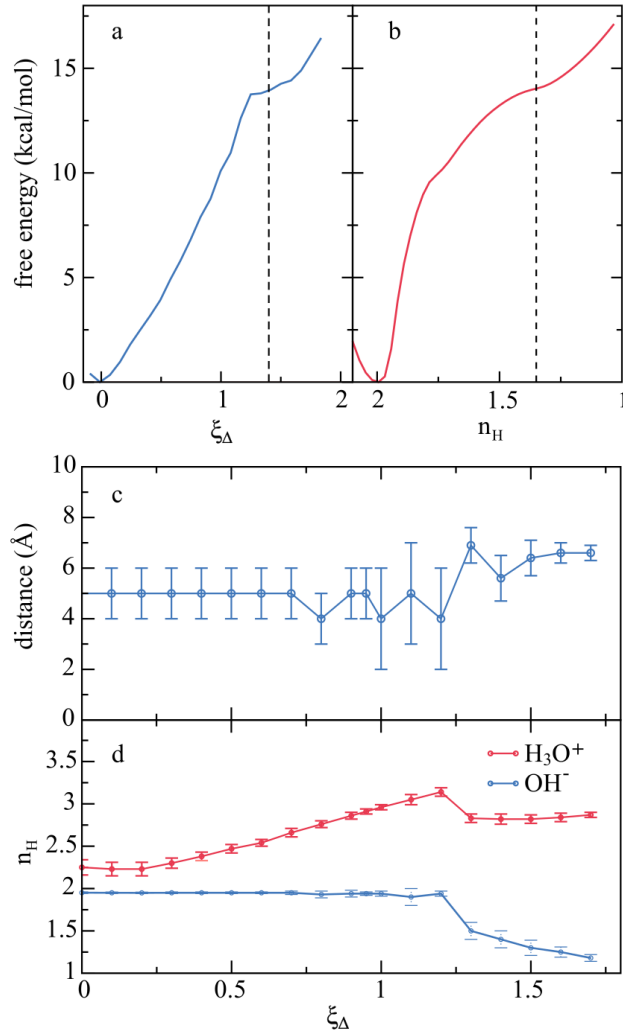


Figure 4. Evolution along the reaction coordinate. **a** and **b**: Free energy profiles for the dissociation of water in the bulk phase, computed with the single-oxygen reaction coordinate n_H (red curve) and with the global reaction coordinate $\xi(\Delta n_H)$ (blue curve). The dashed vertical line marks the reaction endpoint for both coordinates. **c**: Average separation d_{12} between the hydroxide and hydronium species as a function of the global reaction coordinate $\xi(\Delta n_H)$. This separation is defined and computed as the distance between the oxygen atoms exhibiting the maximum and minimum proton coordinations. At the early stages of the reaction, when the proton is still bound to the parent water molecule, the fluctuations of the hydrogen-bond network randomly switch the identity of the minimum coordination oxygen atom, and therefore the value of d_{12} turns out to be an average of all O-O distances in the supercell (~ 5 Å). It is only when the reaction is close to completion that d_{12} achieves the targeted value. **d**: Proton coordination number of the oxygen atoms in the donor (blue) and acceptor (red) water molecules, as a function of the reaction coordinate.

curve in blue, it is first important to identify the reaction endpoint. This can be associated with a value of n_H equal to the coordination number corresponding to free aqueous OH^- in the bulk phase, which, according to our simulations, turns out to be around 1.35 [39]. Figure 4c shows that this coordinate effectively draws the hydroxide and hydronium species apart over the target distance. In Figure 4d, $n_H(1)$ and $n_H(2)$ are plotted as a function of the global reaction coordinate ξ . In particular, $n_H(1)$ reaches a value of 1.35 when $\xi \sim 1.4$, implying that at this point the reaction is complete. In this region the free-energy profile comes to a plateau at an energy that corresponds almost exactly to the value of ΔG_d resulting from the sampling based on the proton coordination of a single oxygen, shown in the same graph. The 2D free-energy surfaces recently reported by Joutsuka shed further light on this discussion: they indicate that, upon dissociation, once the coordination number has reached its final value of ~ 1.3 , the free energy turns out to be quite flat for separations extending between ~ 2.5 and ~ 7 Å [20]. For the model of 256 molecules, a small stabilization, in the order of 1-2 kcal/mol, occurs when the separation increases to 9 Å, concertedly with a rearrangement of the hydrogen bond network. This represents a smooth minimum in the global free-energy landscape which is hard to detect in the smaller models. Aside from this, a modest size dependence was found: the qualitative features of the potential of mean force remained unchanged with respect to the system of 64 molecules, with quantitative differences not larger than 2 kcal/mol [20]. It is to be noticed that the value of n_H corresponding to the free-energy minimum identified in the largest system, of 1.27, is essentially the same that gives the inflection point in Figure 4a. The quality of the free-energy curve produced with our 1D coordinate appears thus comparable to the one resulting from the 2D potential of mean force, but at a much lower computational cost. Yet, as a consequence of the supercell size which prevents from reaching separations beyond ~ 7 Å, this minimum is unseen in our simulations. Whether our 1D reaction coordinate ξ is able to reproduce this minimum for larger sizes will be the subject of future work.

All in all the comparison of the curves in Figures 4a and 4b, along with the 2D free-energy maps presented by Joutsuka, provide two fundamental insights: (i) the spatial decorrelation of the nascent H_3O^+ and OH^- ions contributes a negligible fraction of the overall free energy, meaning that the barrier is dominated by the dissociation step involving breaking the covalent bond that produces the contact ion-pair; (ii) a complete separation of the ions, attainable either through 2D sampling or through the global reaction coordinate ξ , is needed to reach a minimum or at least a metastable region in the free-energy profile, that is not observed with the adoption of a reaction coordinate based on a single oxygen atom.

Further examination of Figure 4d reveals that a gradual protonation of the acceptor H_2O , effected at the expense of the partial dissociation of neighboring molecules, precedes the deprotonation of the donor. The coordination number of the latter, $n_H(1)$, remains approximately constant while the system climbs up the free-energy surface, up to $\xi \sim 1.2$, when it suddenly drops to its endpoint value. Concurrently with this last event, the average separation between the hydroxide and the hydronium species increases by several angstroms. The fluctuations that occur within the hydrogen bond network to facilitate the sequence of events leading to the separation of the contact-ion pair, illustrated in Figure 5a, have been the subject of several previous studies [10, 16] and are in line with the results of ref. [20].

The contribution of the hydrogen bond network beyond the first solvation shell to the self-dissociation of water can be interpreted in terms of the fluctuational correlation functions $C(r)$ based on the fluctuations of the atomic positions. These correlations quantify the entanglement between the dynamics of the incipient ions and that of the water molecules situated at a distance r (see Supporting Information). Figures 5b and

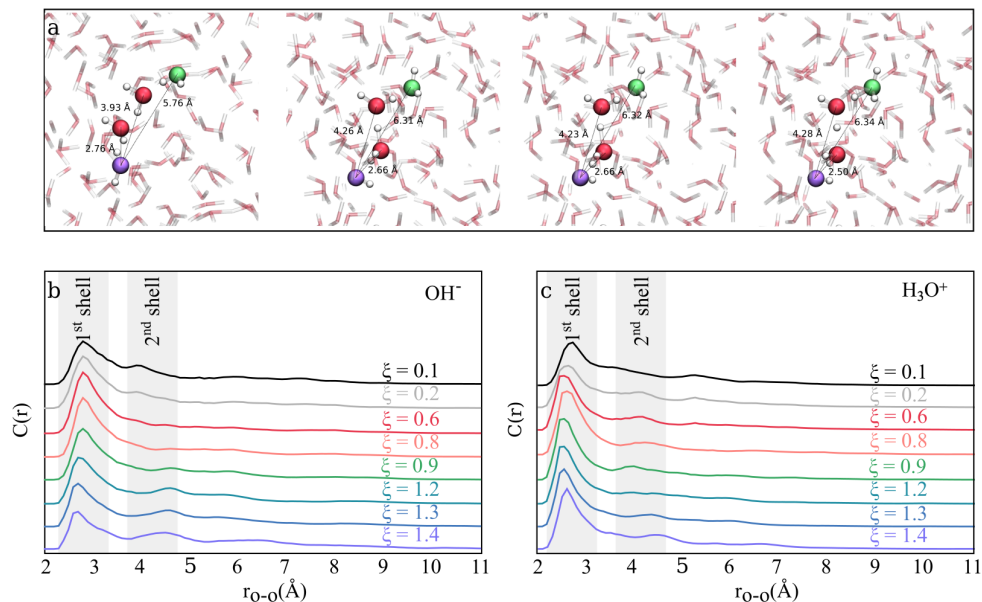


Figure 5. Characterization of the self-dissociation mechanism. **a:** Snapshots selected from umbrella sampling trajectories in the bulk phase, illustrating the dissociation mechanism. Break of the O-H bond leaves a contact ion pair, until a proper alignment of the water wire (depicted in indigo) allows for a barrierless diffusion of the proton via the Grotthuss mechanism. **b:** Fluctuational correlation functions $C(r)$, quantifying the coupling between the dynamics of the nascent OH^- ion and the water molecules placed at r , computed for different values of the global reaction coordinate ξ . **c:** Same as **b** for the H_3O^+ ion.

5c evidence a dynamics of the acceptor and donor water molecules primarily correlated with or influenced by their first solvation shell. As the global coordinate evolves towards the formation of the ions, the relative influence of solvation beyond the first neighbors decreases substantially, reaching a minimum at $\xi \sim 0.6$. At this point, the dynamics of the nascent ions is only coupled to their first solvation layer, independent of the fluctuations taking place further away. For larger values of ξ until completion of the ionization, the second solvation shell slowly regains influence over the ion dynamics (clearly illustrated by the relative fluctuational correlation functions presented in the Supporting Information).

The increasing decoupling between the ions and their second solvation shells during the initial stages of the self-dissociation process attest that the dynamics of the reactants will be largely unaltered by perturbations beyond the closest neighbors. This fact is consistent with the insensitivity of the free-energy profile to size reduction beyond the first shell, reinforcing the mechanism proposed above: the formation of the contact ion pair takes most of the free-energy rise, eventually followed by a barrierless proton diffusion propitiated by a favorable alignment of the hydrogen bond network, manifest in the last part of the mechanism ($\xi \sim 1.3$) where $C(r)$ presents some structure beyond the first neighbors.

Conclusion

Through the application of first-principles biased molecular dynamics simulations combined with an innovative reaction coordinate, the present study conclusively establishes that the dissociation free energy of water is determined by the initial break of the O-H covalent bond. The subsequent separation of the formed ions, via Grotthuss diffusion, entails only a very marginal fraction of the overall energetic cost. As a consequence, in the absence of specific interactions at the interface, the pK_w turns out to be practically invariant with respect to system dimensions, providing that they do not interfere with the solvation of the products. A sizeable drop in K_w will be only seen when the first solvation shell of the ions is not intact, and in particular when the acceptor role of OH⁻ is affected. In clusters, this occurs at some point between $N=6$ and $N=12$. In pores exempt from strong interactions, the primary solvation structure is destabilized in interstices under 1.6 nm, where the accessible space is subnanometric and can hardly accommodate a water bilayer or trilayer with molecules exhibiting a hindered motion. In the slab suspended in the gas phase, of 1 nm width, the translational and orientational freedom of the molecular dipoles is enough to form a first solvation shell around the ions that reinstates the bulk dissociation free energy. In fact, Figure 2b shows that the density profiles for the slab and for the largest pore turn out to be very similar in the inner region. In any case, it is suggestive that the change in the dissociation barrier with respect to size stabilizes when the droplet approaches the length-scale for which hydrogen-bond networks develop, namely, the water hexamer [32,34]. In this way, dissociation free-energy profiles for aqueous clusters or water in nanopores reproduce the behavior corresponding to the bulk phase, with differences only manifesting at subnanometer confinement.

In real chemical systems, it is often not possible to consider size effects separately from interfacial interactions. The presence of charges or polar surface groups, able to establish specific interactions with H₂O and with its ions, will have a disrupting incidence on aqueous reactivity. Many examples can be found in the literature discussing the acceleration or inhibition of reactivity under confinement [7, 13, 24, 35, 50]. Leaving aside physical effects as those examined in refs. [35] and [7], the interactions with the interface appear to be the main factor controlling mechanisms and energetic barriers. Indeed, the present results suggest that when these interactions are not

dominant confinement alone will not affect the chemistry of water independently of the nature of the interface, unless system dimensions become comparable to the molecular size. A broader implication of this finding is that water's self-ionization constant at the hydrophobic air-liquid interface will remain unchanged, warranting further study.

Acknowledgements

We are grateful to Dr. Matias Factorovich and Dr. Mariano Gonzalez Lebrero for useful discussions. This work has been funded by the Agencia Nacional de Promoción Científica y Tecnológica de Argentina (PICT 2016-3167 and PICT 2020-02804). DAS heartily acknowledges the ICTP and its Associates Programme, and the Simons Foundation for support through grant number 284558FY19. AH also acknowledges funding by the European Union (ERC, HyBOP, Grant Number: 101043272). Views and opinions expressed are however those of the author(s) only and do not necessarily reflect those of the European Union or the European Research Council. Neither the European Union nor the granting authority can be held responsible for them.

Conflict of Interest

The authors declare no conflict of interest.

References

- [1] N. Agmon, H. J. Bakker, R. K. Campen, R. H. Henchman, P. Pohl, S. Roke, M. Thämer, and A. Hassanali. Protons and hydroxide ions in aqueous systems. *Chem. Rev.*, 116(13):7642–7672, 2016.
- [2] K. V. Agrawal, S. Shimizu, L. W. Drahushuk, D. Kilcoyne, and M. S. Strano. Observation of extreme phase transition temperatures of water confined inside isolated carbon nanotubes. *Nat. Nanotechnol.*, 12(3):267, 2017.
- [3] A. V. Bandura and S. N. Lvova. The ionization constant of water over wide ranges of temperature and density. *J. Phys. Chem. Ref. Data*, 35:15–30, 2006.
- [4] I. M. Briman, D. Rébiscoul, O. Diat, J.-M. Zanutti, P. Jollivet, P. Barboux, and S. Gin. Impact of pore size and pore surface composition on the dynamics of confined water in highly ordered porous silica. *J. Phys. Chem. C*, 116(12):7021–7028, 2012.
- [5] E. de la Llave, V. Molinero, and D. A. Scherlis. Role of confinement and surface affinity on filling mechanisms and sorption hysteresis of water in nanopores. *J. Phys. Chem. C*, 116(2):1833–1840, 2012.
- [6] T. Dwars, E. Paetzold, and G. Oehme. Reactions in micellar systems. *Angew. Chem. Int. Ed.*, 44:7174–7199, 2005.
- [7] A. Fallah-Araghi, K. Meguellati, J.-C. Baret, A. E. Harrak, T. Mangeat, M. Karplus, S. Ladame, C. M. Marques, and A. D. Griffiths. Enhanced chemical synthesis at soft interfaces: A universal reaction-adsorption mechanism in microcompartments. *Phys. Rev. Lett.*, 112:028301, 2014.
- [8] L. Fumagalli, A. Esfandiar, R. Fabregas, S. Hu, P. Ares, A. Janardanan, Q. Yang, B. Radha, T. Taniguchi, K. Watanabe, G. Gomila, K. S. Novoselov, and A. K.

-
- Geim. Anomalously low dielectric constant of confined water. *Science*, 360(6395):1339–1342, 2018.
- [9] A. Gallo, A. S. F. Farinha, M. Dinis, A.-H. Emwas, A. Santana, R. J. Nielsen, W. A. Goddard, and H. Mishra. The chemical reactions in electrosprays of water do not always correspond to those at the pristine air-water interface. *Chem. Sci.*, 10:2566–2577, 2019.
- [10] P. L. Geissler, C. Dellago, D. Chandler, J. Hutter, and M. Parrinello. Autoionization in liquid water. *Science*, 291:2121–2124, 2001.
- [11] N. Giovambattista, P. J. Rossky, and P. G. Debenedetti. Phase transitions induced by nanoconfinement in liquid water. *Phys. Rev. Lett.*, 102:050603, 2009.
- [12] E. González Solveyra, E. de la Llave, D. A. Scherlis, and V. Molinero. Melting and crystallization of ice in partially filled nanopores. *J. Phys. Chem. B*, 115(48):14196–14204, 2011.
- [13] A. B. Grommet, M. Feller, and R. Klajn. Chemical reactivity under nanoconfinement. *Nat. Nanotechnol.*, 15:256–271, 2020.
- [14] B. Grunberg, T. Emmler, E. Gedat, I. Shenderovich, G. Findenegg, H.-H. Limbach, and G. Buntkowsky. Hydrogen bonding of water confined in mesoporous silica mcm-41 and sba-15 studied by 1h solid-state nmr. *Chem.-Eur. J.*, 10:5689–5696, 2004.
- [15] Y. Hashikawa, S. Hasegawa, and Y. Murata. A single but hydrogen-bonded water molecule confined in an anisotropic subnanospace. *Chem. Commun.*, 54:13686–13689, 2018.
- [16] A. Hassanali, F. Giberti, J. Cuny, T. D. Kühne, and M. Parrinello. Proton transfer through the water gossamer. *P. Natl. Acad. Sci. USA*, page 13723, 2013.
- [17] G. Hummer, J. C. Rasaiah, and J. P. Noworyta. Water conduction through the hydrophobic channel of a carbon nanotube. *Nature*, 414(6860):188, 2001.
- [18] D. Hunt, V. M. Sanchez, and D. A. Scherlis. A quantum-mechanics molecular-mechanics scheme for extended systems. *J. Phys-Condens. Mat.*, 28(33):335201, 2016.
- [19] S. Jahnert, F. Vaca Chavez, G. E. Schaumann, A. Schreiber, M. Schonhoff, and G. H. Findenegg. Melting and freezing of water in cylindrical silica nanopores. *Phys. Chem. Chem. Phys.*, 10:6039–6051, 2008.
- [20] T. Joutsuka. Molecular mechanism of autodissociation in liquid water: Ab initio molecular dynamics simulations. *J. Phys. Chem. B*, 126(24):4565–4571, 2022.
- [21] S. Kittaka, S. Ishimaru, M. Kuranishi, T. Matsuda, and T. Yamaguchi. Enthalpy and interfacial free energy changes of water capillary condensed in mesoporous silica, mcm-41 and sba-15. *Phys. Chem. Chem. Phys.*, 8:3223–3231, 2006.
- [22] N. M. A. Krishnan, B. Wang, G. Falzone, Y. Le Pape, N. Neithalath, L. Pilon, M. Bauchy, and G. Sant. Confined water in layered silicates: The origin of anomalous thermal expansion behavior in calcium-silicate-hydrates. *ACS Appl. Mater. Inter.*, 8(51):35621–35627, 2016.
- [23] A. Küchler, M. Yoshimoto, S. Luginbühl, F. Mavelli, and P. Walde. Enzymatic reactions in confined environments. *Nat. Nanotechnol.*, 11:409–420, 2016.

-
- [24] J. K. Lee, D. Samanta, H. G. Nam, and R. N. Zare. Micrometer-sized water droplets induce spontaneous reduction. *J. Am. Chem. Soc.*, 141:10585–10589, 2019.
- [25] X. Liu, X. Lu, R. Wang, E. J. Meijer, and H. Zhou. Acidities of confined water in interlayer space of clay minerals. *Geochim. Cosmochim. Acta*, 75:4978–4986, 2011.
- [26] E. Mamontov, D. J. Wesolowski, L. Vlcek, P. T. Cummings, J. Rosenqvist, W. Wang, and D. R. Cole. Dynamics of hydration water on rutile studied by backscattering neutron spectroscopy and molecular dynamics simulation. *J. Phys. Chem. C*, 112(32):12334–12341, 2008.
- [27] F. Mikami, K. Matsuda, H. Kataura, and Y. Maniwa. Dielectric properties of water inside single-walled carbon nanotubes. *ACS Nano*, 3(5):1279–1287, 2009.
- [28] S. Mondal and B. Bagchi. Water in carbon nanotubes: Pronounced anisotropy in dielectric dispersion and its microscopic origin. *J. Phys. Chem. Lett.*, 10(20):6287–6292, 2019.
- [29] E. B. Moore, E. de la Llave, K. Welke, D. A. Scherlis, and V. Molinero. Freezing, melting and structure of ice in a hydrophilic nanopore. *Phys. Chem. Chem. Phys.*, 12:4124–4134, 2010.
- [30] M. Moqadam, A. Lervik, E. Riccardi, V. Venkatraman, B. K. Alsberg, and T. S. van Erp. Local initiation conditions for water autoionization. *P. Natl. Acad. Sci. USA*, 115(20):E4569–E4576, 2018.
- [31] D. Muñoz-Santiburcio and D. Marx. Nanoconfinement in slit pores enhances water self-dissociation. *Phys. Rev. Lett.*, 119(5):056002, 2017.
- [32] C. Pérez, M. T. Muckle, D. P. Zaleski, N. A. Seifert, B. Temelso, G. C. Shields, Z. Kisiel, and B. H. Pate. Structures of cage, prism, and book isomers of water hexamer from broadband rotational spectroscopy. *Science*, 336(6083):897–901, 2012.
- [33] T. J. Pinnavaia. Intercalated clay catalysts. *Science*, 220:365–371, 1983.
- [34] J. O. Richardson, C. Pérez, S. Lobsiger, A. A. Reid, B. Temelso, G. C. Shields, Z. Kisiel, D. J. Wales, B. H. Pate, and S. C. Althorpe. Concerted hydrogen-bond breaking by quantum tunneling in the water hexamer prism. *Science*, 351(6279):1310–1313, 2016.
- [35] L. Rubinovich and M. Polak. The intrinsic role of nanoconfinement in chemical equilibrium: Evidence from dna hybridization. *Nano Letters*, 13(5):2247–2251, 2013.
- [36] M. Sattig and M. Vogel. Dynamic crossovers and stepwise solidification of confined water: A 2h nmr study. *J. Phys. Chem. Lett.*, 5(1):174–178, 2014.
- [37] A. Schlaich, E. W. Knapp, and R. R. Netz. Water dielectric effects in planar confinement. *Phys. Rev. Lett.*, 117:048001, 2016.
- [38] A. Schreiber, I. Ketelsen, and G. H. Findenegg. Melting and freezing of water in ordered mesoporous silica materials. *Phys. Chem. Chem. Phys.*, 3:1185–1195, 2001.
- [39] Y. A. P. Sirkin, A. Hassanali, and D. A. Scherlis. One-dimensional confinement inhibits water dissociation in carbon nanotubes. *J. Phys. Chem. Lett.*, 9(17):5029–5033, 2018.

-
- [40] E. G. Solveyra, E. de la Llave, G. J. A. A. Soler-Illia, V. Molinero, and D. A. Scherlis. Structure, dynamics, and phase behavior of water in tio2 nanopores. *J. Phys. Chem. C*, 117(7):3330–3342, 2013.
- [41] M. Sprik. Computation of the pk of liquid water using coordination constraints. *Chem. Phys.*, 258(2):139 – 150, 2000.
- [42] W. Stroberg and S. Schnell. Do cellular condensates accelerate biochemical reactions? lessons from microdroplet chemistry. *Biophys. J.*, 115:3–8, 2018.
- [43] D. Takaiwa, I. Hatano, K. Koga, and H. Tanaka. Phase diagram of water in carbon nanotubes. *P. Natl. Acad. Sci. USA*, 105(1):39–43, 2008.
- [44] B. L. Trout and M. Parrinello. The dissociation mechanism of h₂o in water studied by first-principles molecular dynamics. *Chem. Phys. Lett.*, 288:343–347, 1998.
- [45] A. Tuladhar, S. Dewan, S. Pezzotti, F. Brigiano, F. Creazzo, M.-P. Gaigeot, and E. Borguet. Ions tune interfacial water structure and modulate hydrophobic interactions at silica surfaces. *J. Am. Chem. Soc.*, 142(15):6991–7000, 2020.
- [46] M. I. Velasco, M. B. Franzoni, E. A. Franceschini, E. Gonzalez Solveyra, D. Scherlis, R. H. Acosta, and G. J. A. A. Soler-Illia. Water confined in mesoporous tio2 aerosols: Insights from nmr experiments and molecular dynamics simulations. *J. Phys. Chem. C*, 121(13):7533–7541, 2017.
- [47] Z. Wei, Y. Li, R. G. Cooks, and X. Yan. Accelerated reaction kinetics in microdroplets: Overview and recent developments. *Annu. Rev. Phys. Chem.*, 71:31–51, 2020.
- [48] T. Werder, J. H. Walther, R. L. Jaffe, T. Halicioglu, and P. Koumoutsakos. On the water carbon interaction for use in molecular dynamics simulations of graphite and carbon nanotubes. *J. Phys. Chem. B*, 107(6):1345–1352, 2003.
- [49] S. Xu, G. W. Scherer, T. S. Mahadevan, and S. H. Garofalini. Thermal expansion of confined water. *Langmuir*, 25(9):5076–5083, 2009.
- [50] X. Yan, R. M. Bain, and R. G. Cooks. Organic reactions in microdroplets: Reaction acceleration revealed by mass spectrometry. *Angew. Chem. Int. Ed.*, 55:2–15, 2016.
- [51] T. Zelovich and M. E. Tuckerman. Water layering affects hydroxide diffusion in functionalized nanoconfined environments. *J. Phys. Chem. Lett.*, 11(13):5087–5091, 2020.
- [52] J. Zhong, M. Kumar, J. S. Francisco, and X. C. Zeng. Insight into chemistry on cloud/aerosol water surfaces. *Acc. Chem. Res.*, 51(5):1229–1237, 2018.